New Journal of Physics
The open-access journal for physics

Dissipation in circuit quantum electrodynamics: lasing and cooling of a low-frequency oscillator

Julian Hauss[1,2], Arkady Fedorov[1,3], Stephan André[1], Valentina Brosco[1], Carsten Hutter[1,4], Robin Kothari[1,5], Sunil Yeshwanth[1,6], Alexander Shnirman[7,8,9] and Gerd Schön[1,8]

[1] Institut für Theoretische Festkörperphysik, Universität Karlsruhe, D-76128 Karlsruhe, Germany
[2] Lichttechnisches Institut, Universität Karlsruhe, D-76128 Karlsruhe, Germany
[3] Kavli Institute of Nanoscience, Delft University of Technology, 2600 GA Delft, The Netherlands
[4] Department of Physics, Stockholm University, AlbaNova University Center, SE-106 91 Stockholm, Sweden
[5] Department of Physics, Indian Institute of Technology Bombay, Mumbai 400076, India
[6] Department of Physics, Indian Institute of Technology, Kanpur 208016, India
[7] Institut für Theorie der Kondensierten Materie, Universität Karlsruhe, D-76128 Karlsruhe, Germany
[8] DFG-Center for Functional Nanostructures (CFN), Universität Karlsruhe, D-76128 Karlsruhe, Germany
E-mail: shnirman@tkm.uni-karlsruhe.de

New Journal of Physics **10** (2008) 095018 (17pp)
Received 5 June 2008
Published 30 September 2008
Online at http://www.njp.org/
doi:10.1088/1367-2630/10/9/095018

Abstract. Superconducting qubits coupled to electric or nanomechanical resonators display effects previously studied in quantum electrodynamics (QED) as well as extensions thereof. Here, we consider a driven qubit coupled to a low-frequency oscillator and study the influence of dissipation. When the qubit is driven to perform Rabi oscillations, with Rabi frequency in resonance with the oscillator, the latter can be driven far from equilibrium. Blue detuned driving leads to a population inversion in the qubit and lasing behavior of the oscillator ('single-atom laser'). For red detuning, the qubit cools the oscillator. This behavior persists at the symmetry point where the qubit–oscillator coupling is quadratic and decoherence effects are minimized. Here, the system realizes a 'single-atom-two-photon laser'.

[9] Author to whom any correspondence should be addressed.

© IOP Publishing Ltd and Deutsche Physikalische Gesellschaft

Contents

1. Introduction

Recent experiments on quantum state engineering with superconducting circuits realized concepts originally introduced in the field of quantum optics, as well as extensions thereof, e.g. to the regime of strong coupling [1]–[8]. Josephson qubits play the role of two-level atoms, whereas electric or nanomechanical oscillators play the role of the quantized radiation field. These 'circuit quantum electrodynamics (QED)' experiments prompted substantial theoretical activities [9]–[19]. In most QED or circuit QED experiments, the atom or qubit transition frequency is near resonance with the oscillator. In contrast, in the experiments of [1], with setup shown in figure 1(a), the qubit is coupled to a slow LC tank circuit with frequency ($\omega_T/2\pi \sim$ MHz) much lower than the qubit's level splitting ($\Delta E/2\pi\hbar \sim 10$ GHz). The idea of this experiment is to drive the qubit to perform Rabi oscillations with Rabi frequency in resonance with the oscillator, $\Omega_R \approx \omega_T$. In this situation, the driven qubit should excite the oscillator, and indeed in the experiments a substantial enhancement of the amplitude of the oscillator was observed [1].

Initial attempts to explain the effect did not resolve several issues [20, 21]. In the experiments, in order to minimize decoherence effects, the Josephson flux qubit was biased near the flux degeneracy point. At this symmetry point also the coupling to the oscillator is tuned to zero, and the enhancement should vanish. Uncontrolled small deviations from the symmetry point might lead to the observed effect [1, 20], but this explanation was not supported by experiments. Here, we explore an alternative, namely that a quadratic coupling to the oscillator near the resonance condition $\Omega_R \approx 2\omega_T$ is responsible for the observed enhancement. In the following, we will consider both linear as well as quadratic coupling, which dominate away from the symmetry point and at this point, respectively.

The second unresolved problem is the magnitude of the effect. The experiments [1] showed an increase by a factor of 4–5 in the amplitude, i.e. 16–25 in the number of oscillator quanta. The theory of [20], valid in the perturbative regime, predicts a much weaker effect. We obtain a strong effect as follows [18]: for blue detuning of the qubit driving, a population inversion is created in the qubit at the Rabi frequency, and at the resonance $\Omega_R \approx \omega_T$ the system becomes a 'single-atom laser', or for $\Omega_R \approx 2\omega_T$ a 'single-atom-two-photon laser' [22, 23]. In both cases, the lasing instability is reached for realistic system parameters. In this state, the oscillator

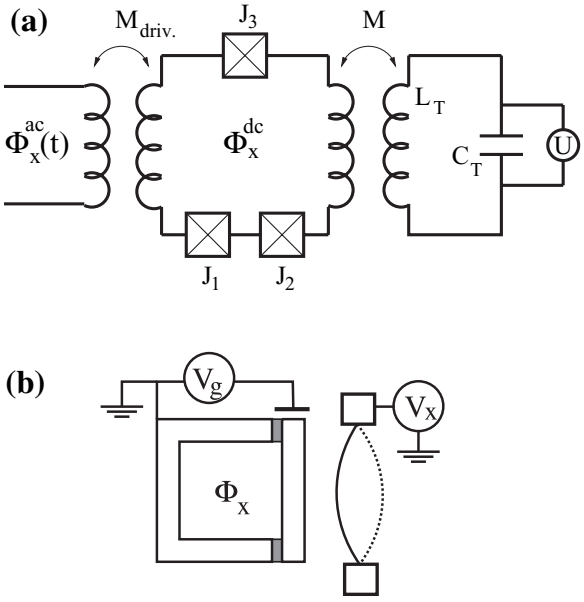

Figure 1. (a) In the setup of [1], an externally driven three-junction flux qubit is coupled inductively to an LC oscillator. (b) A charge qubit is coupled capacitively to a mechanical resonator.

no longer responds linearly to external perturbations (its effective friction constant becomes negative), and the number of quanta in the oscillator increases strongly until saturation is reached due to nonlinear effects. The analysis of the driven circuit QED system shows that its properties depend strongly on relaxation and decoherence effects in the qubit.

A related situation, called 'dressed-state lasing', had been studied before in quantum optics [24]–[26]. The present scenario differs from that one in so far as the resonator modes are coupled to the low-frequency Rabi oscillations rather than to the high-frequency Mollow transitions. The Rabi frequency can be readily tuned to resonance with the oscillator, which should facilitate reaching the lasing threshold and a proper lasing state. The unusual resonance condition has also been explored in [27] in connection with coupling of atoms.

For red detuning of the qubit driving, the qubit should cool the oscillator [18]. A similar strategy for cooling of a nanomechanical resonator via a Cooper pair box qubit has been recently suggested in [28].

Also in situations where the qubit, e.g. a Josephson charge qubit, is coupled to a nanomechanical oscillator (figure 1(b)) it either cools or amplifies the oscillator. On one hand, this provides an important tool on the way to ground state cooling, on the other hand, it provides a realization of what is called a SASER [29].

Lasing and cooling of the oscillator have also been observed in a slightly different setup, when the Rabi-driven qubit is replaced by a superconducting single-electron transistor (SSET) biased near the Josephson quasiparticle cycle [30]–[32]. Coupled to a nanomechanical or an electric oscillator, the SSET can be used to either cool the oscillator [33]–[38] or to produce laser-like behavior. The latter has been demonstrated recently in the experiments of Astafiev *et al* [39].

The present paper is organized as follows. In the following section, the system of driven qubit coupled to a low-frequency oscillator is introduced and analyzed theoretically using the

appropriate rotating wave approximations (RWAs) and the Schrieffer–Wolf transformation. We thus arrive at an effective Hamiltonian of the system, which allows us to proceed using techniques from quantum optics. We then consider dissipation in the rotating frame and show that it plays a crucial role for the lasing state. In particular, we formulate the master equation, which forms the basis for a numerical analysis. Finally, we derive the Langevin equations describing the dynamics of the oscillator in the presence of the driven qubit. In the next section, we present the results of the numerical analysis of the Langevin equations as well as of the full master equation and interpret them in terms of lasing with or without bistability and cooling. The paper concludes with a discussion covering several extensions.

2. Theory

2.1. The Hamiltonian

The systems to be considered are shown in figure 1. A qubit is coupled to an oscillator and driven to perform Rabi oscillations. To be specific, we first analyze a flux qubit coupled to an electric oscillator (figure 1(a)) with Hamiltonian

$$H = -\tfrac{1}{2}\,\epsilon\left(\Phi_x^{\rm dc}\right)\sigma_z - \tfrac{1}{2}\,\Delta\sigma_x - \hbar\Omega_{\rm R0}\cos(\omega_{\rm d}t)\,\sigma_z + \hbar\omega_{\rm T}\,a^\dagger a + g\,\sigma_z\left(a + a^\dagger\right). \quad (1)$$

The first two terms describe the qubit, with Pauli matrices $\sigma_{x,z}$ operating in the flux basis of the qubit. The energy bias between the flux states $\epsilon(\Phi_x^{\rm dc})$ is controlled by an external dc magnetic flux $\Phi_x^{\rm dc}$, and Δ is the tunneling amplitude between the basis states. The resulting level spacing $\Delta E \equiv \sqrt{\epsilon^2 + \Delta^2}$ typically lies in the range of several GHz. The third term accounts for the driving of the qubit by an applied ac magnetic flux with amplitude $\Omega_{\rm R0}$ and frequency $\omega_{\rm d}$. The last two terms describe the oscillator with frequency $\omega_{\rm T} = 1/\sqrt{L_{\rm T}C_{\rm T}}$ as well as the qubit–oscillator interaction. In the experiments of [1], $\omega_{\rm T}$ lies in the range of several 10 MHz, whereas the coupling constant $g \approx M I_{\rm p} I_{\rm T,0}$ is of the order of 10 MHz. Here M is the mutual inductance, $I_{\rm p}$ the magnitude of the persistent current in the qubit, and $I_{\rm T,0} = \sqrt{\hbar\omega_{\rm T}/2L_{\rm T}}$ the amplitude of the vacuum fluctuation of the current in the LC oscillator.

After transformation to the eigenbasis of the qubit, which is the natural basis for the description of the dissipation, the Hamiltonian reads

$$H = -\tfrac{1}{2}\Delta E\sigma_z - \hbar\Omega_{\rm R0}\cos(\omega_{\rm d}t)\,(\sin\zeta\,\sigma_z - \cos\zeta\,\sigma_x) + \hbar\omega_{\rm T}\,a^\dagger a + g\,(\sin\zeta\,\sigma_z - \cos\zeta\,\sigma_x)\left(a + a^\dagger\right), \quad (2)$$

with $\tan\zeta = \epsilon/\Delta$ and $\Delta E \equiv \sqrt{\epsilon^2 + \Delta^2}$.

Because of the large difference of the energy scales between the qubit and the oscillator, $\Delta E \gg \hbar\omega_{\rm T}$, it is tempting, in the spirit of the usual RWA, to drop the transverse coupling term $-g\cos\zeta\,\sigma_x(a + a^\dagger)$ of equation (2). However, near the symmetry point (where $\sin\zeta = 0$) the longitudinal coupling is weak. Therefore, we retain the transverse coupling, but transform it by employing a Schrieffer–Wolff transformation, $U_{\rm S} = \exp({\rm i}S)$, with generator $S = (g/\Delta E)\cos\zeta\,(a + a^\dagger)\,\sigma_y$, into a second-order longitudinal coupling. On the other hand, since $\hbar\omega_{\rm d} \sim \Delta E$, we can drop within RWA the longitudinal driving term $-\hbar\Omega_{\rm R0}\cos(\omega_{\rm d}t)\sin\zeta\,\sigma_z$. The Hamiltonian then reads

$$H = -\tfrac{1}{2}\,\Delta E\,\sigma_z + \hbar\Omega_{\rm R0}\cos(\omega_{\rm d}t)\cos\zeta\,\sigma_x + \hbar\omega_{\rm T}\,a^\dagger a + g\sin\zeta\,\sigma_z\left(a + a^\dagger\right) - \frac{g^2}{\Delta E}\cos^2\zeta\,\sigma_z\left(a + a^\dagger\right)^2. \quad (3)$$

A further unitary transformation with $U_{\rm R} = \exp(-{\rm i}\omega_{\rm d}\sigma_z t/2)$ brings the Hamiltonian to the rotating frame, $\tilde{H} \equiv U_{\rm R} H U_{\rm R}^{\dagger} + {\rm i}\hbar \dot{U}_{\rm R} U_{\rm R}^{\dagger}$, with

$$\tilde{H} = \tfrac{1}{2}\hbar\delta\omega\,\sigma_z + \tfrac{1}{2}\hbar\Omega_{\rm R0}\,\cos\zeta\,\sigma_x + \hbar\omega_{\rm T}\,a^{\dagger}a + g\sin\zeta\,\sigma_z\left(a+a^{\dagger}\right) - \tfrac{g^2}{\Delta E}\cos^2\zeta\,\sigma_z\left(a+a^{\dagger}\right)^2. \tag{4}$$

Here $\delta\omega \equiv \omega_{\rm d} - \Delta E/\hbar$ is the detuning. After diagonalization of the qubit terms, we obtain

$$\tilde{H} = \frac{1}{2}\hbar\Omega_{\rm R}\,\sigma_z + \hbar\omega_{\rm T}\,a^{\dagger}a + g\sin\zeta\,\left[\sin\beta\,\sigma_z - \cos\beta\,\sigma_x\right]\left(a+a^{\dagger}\right) - \frac{g^2}{\Delta E}\cos^2\zeta\,\left[\sin\beta\,\sigma_z - \cos\beta\,\sigma_x\right]\left(a+a^{\dagger}\right)^2, \tag{5}$$

with $\Omega_{\rm R} = \sqrt{\Omega_{\rm R0}^2\cos^2\zeta + \delta\omega^2}$ and $\tan\beta = \delta\omega/(\Omega_{\rm R0}\cos\zeta)$.

Finally, we employ a second RWA. While the first one dropped counter-rotating terms with frequencies of order $\Delta E/\hbar$, the second one drops terms oscillating with Rabi frequency $\Omega_{\rm R}$ or the oscillator frequency $\omega_{\rm T}$. This (second RWA) approximation will be justified below. In the interaction representation with respect to the non-interacting Hamiltonian, $\tilde{H}_0 = (\hbar\Omega_{\rm R}/2)\sigma_z + \hbar\omega_{\rm T}a^{\dagger}a$, we finally arrive at

$$\tilde{H}_{\rm I} = g_1\left(a^{\dagger}\sigma_- {\rm e}^{-{\rm i}(\Omega_{\rm R}-\omega_{\rm T})t} + {\rm h.c.}\right) + g_2\left(a^{\dagger 2}\sigma_- {\rm e}^{-{\rm i}(\Omega_{\rm R}-2\omega_{\rm T})t} + {\rm h.c.}\right) + g_3\left(a^{\dagger}a + aa^{\dagger}\right)\sigma_z. \tag{6}$$

We kept both single-photon and two-photon interactions, with $g_1 = -g\sin\zeta\cos\beta$ and $g_2 = (g^2/\Delta E)\cos^2\zeta\cos\beta$, although within RWA only one of them survives, i.e. the single-photon term for $\Omega_{\rm R} \sim \omega_{\rm T}$, or the two-photon term for $\Omega_{\rm R} \sim 2\omega_{\rm T}$. The last term of (6) with $g_3 = -(g^2/\Delta E)\cos^2\zeta\sin\beta$ is the ac-Stark effect, causing a qubit-state-dependent frequency shift of the oscillator [40]. In what follows, we will assume that the qubit is kept near the symmetry point, i.e. $\epsilon \ll \Delta$ and $\cos\zeta \approx 1$.

2.2. Transition rates in the rotation frame

The transformation to 'dressed states' in the rotating frame modifies the relaxation, excitation and decoherence rates as compared to the standard results [41, 42]. To illustrate these effects and justify the treatment of the dissipation in later sections, we first consider a driven qubit (ignoring the coupling to the resonator) coupled to a bath observable $\hat{X}$,

$$H = -\tfrac{1}{2}\Delta E\,\sigma_z + \hbar\Omega_{\rm R0}\,\cos(\omega_{\rm d}t)\,\sigma_x - \tfrac{1}{2}\left(b_x\sigma_x + b_y\sigma_y + b_z\sigma_z\right)\hat{X} + H_{\rm bath}. \tag{7}$$

In the absence of driving, $\Omega_{\rm R0} = 0$, and for regular (i.e. smooth as a function of the frequency) power spectra of the fluctuating bath observables, we can proceed using golden rule-type arguments [41, 42]. The transverse noise, coupling to σ_x and σ_y, is responsible for relaxation and excitation processes with rates

$$\begin{aligned}\Gamma_{\downarrow} &= \frac{|b_{\perp}|^2}{4\hbar^2}\langle\hat{X}^2\rangle_{\omega=\Delta E},\\ \Gamma_{\uparrow} &= \frac{|b_{\perp}|^2}{4\hbar^2}\langle\hat{X}^2\rangle_{\omega=-\Delta E},\end{aligned} \tag{8}$$

whereas longitudinal noise, coupling to σ_z, produces a pure dephasing with rate

$$\Gamma_{\varphi}^{*} = \frac{|b_z|^2}{2\hbar^2}S_X(\omega=0). \tag{9}$$

Here $b_\perp \equiv b_x + \mathrm{i}b_y$, and we introduced the ordered correlation function $\langle \hat{X}^2 \rangle_\omega \equiv \int \mathrm{d}t \mathrm{e}^{\mathrm{i}\omega t} \langle \hat{X}(t)\hat{X}(0) \rangle$, as well as the power spectrum, i.e. the symmetrized correlation function, $S_X(\omega) \equiv (\langle \hat{X}^2 \rangle_\omega + \langle \hat{X}^2 \rangle_{-\omega})/2$. The rates (8) and (9) also define the relaxation rate $1/T_1 = \Gamma_1 = \Gamma_\downarrow + \Gamma_\uparrow$ and the total dephasing rate $1/T_2 = \Gamma_\varphi = \Gamma_1/2 + \Gamma_\varphi^*$, which appear in the Bloch equations for the qubit.

To account for the driving with frequency ω_d, it is convenient to transform to the rotating frame via a unitary transformation $U_\mathrm{R} = \exp(-\mathrm{i}\omega_\mathrm{d}\sigma_z t/2)$. Within RWA, the transformed Hamiltonian reduces to

$$\tilde{H} = \tfrac{1}{2}\hbar \left[\Omega_{\mathrm{R}0}\sigma_x + \delta\omega\sigma_z\right] + H_\mathrm{bath} - \tfrac{1}{2}\left[b_z\sigma_z + b_\perp \mathrm{e}^{\mathrm{i}\omega_\mathrm{d}t}\sigma_- + b_\perp^* \mathrm{e}^{-\mathrm{i}\omega_\mathrm{d}t}\sigma_+\right]\hat{X}, \tag{10}$$

with detuning $\delta\omega \equiv \omega_\mathrm{d} - \Delta E/\hbar$. The RWA cannot be used in the second line of (10), since the fluctuations $\hat{X}$ contain potentially all frequencies, including those of order $\pm\omega_\mathrm{d}$, which can compensate fast oscillations.

Diagonalizing the first term of (10) one obtains

$$\begin{aligned}\tilde{H} = \frac{1}{2}\hbar\Omega_\mathrm{R}\,\sigma_z + H_\mathrm{bath} - \left[\frac{\sin\beta}{2}\,b_z + \frac{\cos\beta}{4}\,(b_\perp^*\,\mathrm{e}^{-\mathrm{i}\omega_\mathrm{d}t} + b_\perp\,\mathrm{e}^{\mathrm{i}\omega_\mathrm{d}t})\right]\sigma_z\,\hat{X} \\ - \left\{\left[\frac{(\sin\beta+1)}{4}\,b_\perp^*\,\mathrm{e}^{-\mathrm{i}\omega_\mathrm{d}t} + \frac{(\sin\beta-1)}{4}\,b_\perp\,\mathrm{e}^{\mathrm{i}\omega_\mathrm{d}t} - \frac{\cos\beta}{2}\,b_z\right]\sigma_+\,\hat{X} + \mathrm{h.c.}\right\},\end{aligned} \tag{11}$$

with $\Omega_\mathrm{R} = \sqrt{\Omega_{\mathrm{R}0}^2 + \delta\omega^2}$ and $\tan\beta = \delta\omega/\Omega_{\mathrm{R}0}$.

From here golden rule arguments yield the relaxation and excitation rates in the rotating frame [43]

$$\begin{aligned}\tilde{\Gamma}_\downarrow &\approx \frac{b_z^2}{4\hbar^2}\cos^2\beta\,\langle\hat{X}^2\rangle_{\Omega_\mathrm{R}} + \frac{|b_\perp|^2}{16\hbar^2}\left[(1-\sin\beta)^2\,\langle\hat{X}^2\rangle_{\omega_\mathrm{d}+\Omega_\mathrm{R}} + (1+\sin\beta)^2\,\langle\hat{X}^2\rangle_{-\omega_\mathrm{d}+\Omega_\mathrm{R}}\right], \\ \tilde{\Gamma}_\uparrow &\approx \frac{b_z^2}{4\hbar^2}\cos^2\beta\,\langle\hat{X}^2\rangle_{-\Omega_\mathrm{R}} + \frac{|b_\perp|^2}{16\hbar^2}\left[(1-\sin\beta)^2\,\langle\hat{X}^2\rangle_{-\omega_\mathrm{d}-\Omega_\mathrm{R}} + (1+\sin\beta)^2\,\langle\hat{X}^2\rangle_{\omega_\mathrm{d}-\Omega_\mathrm{R}}\right],\end{aligned} \tag{12}$$

as well as the 'pure' dephasing rate [43]

$$\tilde{\Gamma}_\varphi^* \approx \frac{b_z^2}{2\hbar^2}\sin^2\beta\,S_X(\omega=0) + \frac{|b_\perp|^2}{4\hbar^2}\cos^2\beta\,S_X(\omega_\mathrm{d}). \tag{13}$$

We note the effect of the frequency mixing, and due to the diagonalization the effects of longitudinal and transverse noise on relaxation and decoherence get mixed. In addition, we note that the rates also depend on the fluctuations' power spectrum at the Rabi frequency, $\langle\hat{X}^2\rangle_{\pm\Omega_\mathrm{R}}$.

For a sufficiently regular power spectrum of the fluctuations at frequencies $\omega \approx \pm\Delta E/\hbar$, we can ignore the effect of detuning and the small shifts by $\pm\Omega_\mathrm{R}$ as compared to the high frequency $\omega_\mathrm{d} \approx \Delta E/\hbar$. We further assume that $\Omega_\mathrm{R} \ll kT/\hbar$. In this case, we find the simple relations

$$\begin{aligned}\tilde{\Gamma}_\uparrow &= \frac{(1+\sin\beta)^2}{4}\,\Gamma_\downarrow + \frac{(1-\sin\beta)^2}{4}\,\Gamma_\uparrow + \frac{1}{2}\cos^2\beta\,\Gamma_\nu, \\ \tilde{\Gamma}_\downarrow &= \frac{(1-\sin\beta)^2}{4}\,\Gamma_\downarrow + \frac{(1+\sin\beta)^2}{4}\,\Gamma_\uparrow + \frac{1}{2}\cos^2\beta\,\Gamma_\nu, \\ \tilde{\Gamma}_\varphi^* &= \sin^2\beta\,\Gamma_\varphi^* + \frac{\cos^2\beta}{2}(\Gamma_\downarrow + \Gamma_\uparrow),\end{aligned} \tag{14}$$

where the rates in the lab frame are given by equation (8) and the new rate, $\Gamma_\nu \equiv \frac{1}{2\hbar^2} b_z^2 S_X(\Omega_R)$, depends on the power spectrum at the Rabi frequency.

To proceed, we concentrate on the regime relevant for our system. At low temperatures, $k_B T \ll \Delta E \approx \hbar\omega_d$, we can neglect $\Gamma_\uparrow$ as it is exponentially small. We also assume that the system is tuned near the symmetry point of the qubit, where $b_z \approx 0$. More precisely, we assume that Γ_ν can be neglected as compared to $\Gamma_\downarrow$. Even if very strong $1/f$ noise causes substantial pure dephasing at and near the symmetry point, the rate Γ_ν depends on the noise power spectrum at the frequency Ω_R which is usually higher than the characteristic frequencies of the $1/f$ noise. Thus we can safely neglect Γ_ν and we are left with

$$\tilde{\Gamma}_{\downarrow/\uparrow} \approx \frac{(1 \mp \sin\beta)^2}{4}\,\Gamma_0, \quad \tilde{\Gamma}_\varphi^* \approx \frac{\cos^2\beta}{2}\,\Gamma_0, \tag{15}$$

where

$$\Gamma_0 \equiv \frac{|b_\perp|^2}{4\hbar^2}\langle \hat{X}^2\rangle_{\omega=\Delta E/\hbar} = \Gamma_\downarrow. \tag{16}$$

The ratio of up- and down-transitions depends on the detuning and can be expressed by an effective temperature. Right on resonance, where $\beta = 0$, we have $\tilde{\Gamma}_\uparrow = \tilde{\Gamma}_\downarrow$, corresponding to infinite temperature or a classical drive. For 'blue' detuning, $\beta > 0$, we find $\tilde{\Gamma}_\uparrow > \tilde{\Gamma}_\downarrow$, i.e. *negative temperature*. This leads to a population inversion of the qubit, which is the basis for the lasing behavior which will be described below.

In a more careful analysis, not making use of the 'white noise' approximation, we obtain for $\beta = 0$

$$\frac{\tilde{\Gamma}_\downarrow}{\tilde{\Gamma}_\uparrow} = \frac{\langle \hat{X}^2\rangle_{\omega_d+\Omega_R}}{\langle \hat{X}^2\rangle_{\omega_d-\Omega_R}}. \tag{17}$$

For example, for Ohmic noise and low bath temperature this reduces to $\tilde{\Gamma}_\downarrow/\tilde{\Gamma}_\uparrow \approx 1 + 2\Omega_R/\omega_d$, which corresponds to an effective temperature of order $2\hbar\omega_d/k_B \approx 2\Delta E/k_B$, which by assumption is high but finite. The infinite temperature threshold is crossed toward negative temperatures at weak blue detuning when the condition

$$\frac{(1+\sin\beta)^2}{(1-\sin\beta)^2} \sim 1 + \frac{2\Omega_R}{\omega_d} \tag{18}$$

is satisfied. We note that all qualitative features are well reproduced by the approximation (15).

To illustrate how the population inversion is created for blue detuning we show in figure 2 the level structure, i.e. the formation of dressed states, of a near-resonantly driven qubit. For the purpose of this explanation the driving field is quantized. This level structure was described first by Mollow [25]. The picture also illustrates how for blue detuning a pure relaxation process, $\Gamma_\downarrow = \Gamma_0$, in the laboratory frame predominantly leads to an excitation process, $\tilde{\Gamma}_\uparrow$, in the rotating frame.

2.3. The Liouville equation in the rotating frame

Within the approximation leading to the rates (14) the Liouville equation governing the dynamics of the density matrix in the rotating frame and in the interaction representation with respect to $\tilde{H}_0$ can be presented in a simple Lindblad form,

$$\dot{\tilde{\rho}} = -\frac{\mathrm{i}}{\hbar}\left[\tilde{H}_I, \tilde{\rho}\right] + \tilde{L}_Q\tilde{\rho} + L_R\tilde{\rho}, \tag{19}$$

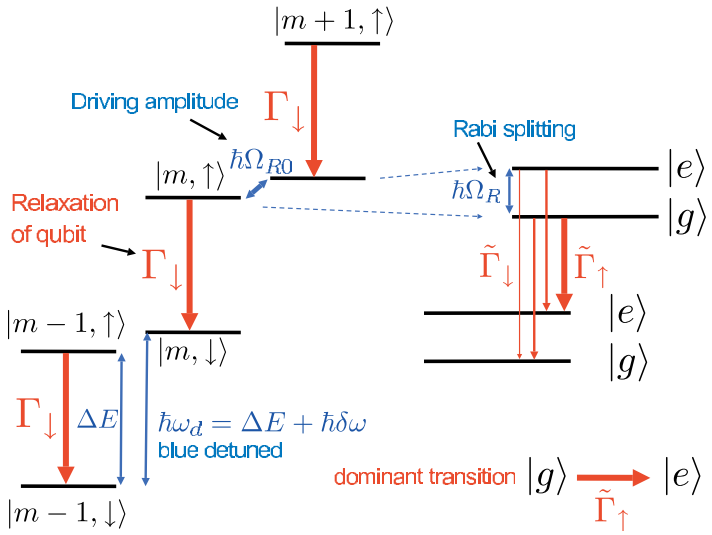

Figure 2. Relaxation rates in the basis of the dressed states. The left staircase denotes the eigenstates of the undriven qubit, $|\uparrow\rangle, |\downarrow\rangle$ and of the (quantized) driving field, $|m\rangle$, before the driving is switched on, i.e. for $\Omega_{R0} = 0$. The Hamiltonian in this basis is obtained from (3) by replacing $\hbar\Omega_{R0}\cos\omega_d t$ with $\lambda(d^\dagger + d)$, where λ is the coupling constant between the qubit and the driving field and d and $d^\dagger$ are the annihilation and the creation operators of the driving field. The right staircase stands for the dressed states of a driven qubit near resonance. They are obtained by, e.g. diagonalization (blue dashed lines) of the 2×2 Hamiltonian which couples the states $|m,\uparrow\rangle$ and $|m+1,\downarrow\rangle$. This gives $|g\rangle = \cos(\frac{\pi}{4} - \frac{\beta}{2})|m,\uparrow\rangle + \sin(\frac{\pi}{4} - \frac{\beta}{2})|m+1,\downarrow\rangle$ and $|e\rangle = -\sin(\frac{\pi}{4} - \frac{\beta}{2})|m,\uparrow\rangle + \cos(\frac{\pi}{4} - \frac{\beta}{2})|m+1,\downarrow\rangle$. The bare Rabi frequency is given by $\Omega_{R0} \approx \lambda\sqrt{\bar{m}}$, where $\bar{m}$ is the average number of photons in the coherent (classical) driving field. The red arrows stand for relaxation rates. All rates are directed down in energy, since only the relaxation $\Gamma_\downarrow$ is considered. However, in the dressed states basis, the dominant rate is from the state $|g\rangle$ to the state $|e\rangle$, i.e. an inversion takes place.

where $\tilde{\rho}$ is the density matrix in the rotating frame in the interaction representation. The qubit dissipation is described by

$$\tilde{L}_Q\tilde{\rho} = \frac{\tilde{\Gamma}_\downarrow}{2}(2\sigma_-\tilde{\rho}\sigma_+ - \tilde{\rho}\sigma_+\sigma_- - \sigma_+\sigma_-\tilde{\rho}) + \frac{\tilde{\Gamma}_\uparrow}{2}(2\sigma_+\tilde{\rho}\sigma_- - \tilde{\rho}\sigma_-\sigma_+ - \sigma_-\sigma_+\tilde{\rho}) + \frac{\tilde{\Gamma}^*_\varphi}{2}(\sigma_z\tilde{\rho}\sigma_z - \tilde{\rho})\,. \tag{20}$$

It has the same form as in the lab frame, except that the rates are those appropriate for the rotating frame. Within the approximations leading to the rates (15), the master equation (19) can be obtained from the master equation in the lab frame by performing the transformations outlined above for the Hamiltonian. The resonator damping, with strength parametrized by κ, can be written as [44]

$$L_R\tilde{\rho} = \frac{\kappa}{2}(N_{th}+1)\left(2a\tilde{\rho}a^\dagger - a^\dagger a\tilde{\rho} - \rho a^\dagger a\right) + \frac{\kappa}{2}N_{th}\left(2a^\dagger\tilde{\rho}a - aa^\dagger\tilde{\rho} - \tilde{\rho}aa^\dagger\right). \tag{21}$$

Here $N_{th} = 1/[\exp(\hbar\omega_T/kT) - 1]$ is the thermal photon number in the resonator.

Since we consider qubits with high degree of coherence, we are motivated to study the regime $\Gamma_0, \kappa, g_1, g_2, g_3 \ll \omega_T, \Omega_R$, where the second RWA performed above with respect to frequencies ω_T, Ω_R is justified (from now on we set $\hbar = 1$).

2.4. The single-qubit laser

In the following we will consider two resonance situations, when the Rabi frequency is in resonance with the oscillator, $\Omega_R \approx \omega_T$, or when $\Omega_R \approx 2\omega_T$. In these cases either the one- or the two-photon interactions dominate. We will study the effects of detuning of the Rabi frequency Ω_R relative to that of the oscillator. We will also investigate the effects of blue or red detuning of the qubit driving frequency, $\delta\omega \equiv \omega_d - \Delta E$.

2.4.1. One-photon interaction. Near the resonance condition, $\Omega_R \approx \omega_T$, the Hamiltonian (6) in RWA reduces to

$$H_I = g_1 \left(a^\dagger \sigma_- e^{-i(\Omega_R - \omega_T)t} + \text{h.c.}\right) + g_3 \left(a^\dagger a + a a^\dagger\right) \sigma_z. \tag{22}$$

From here we can proceed in the frame of the standard semiclassical approach [44, 45] of laser physics with the following main steps: in the absence of fluctuations, the system is described by Maxwell–Bloch equations for the classical variables $\alpha = \langle a \rangle$, $\alpha^* = \langle a^\dagger \rangle$, $s_\pm = \langle \sigma_\pm \rangle$ and $s_z = \langle \sigma_z \rangle$, which can be derived from the Hamiltonian (22) if all correlation functions are assumed to factorize. Next the qubit variables can be adiabatically eliminated as long as $\kappa,\ g_1 \ll \tilde{\Gamma}_1, \tilde{\Gamma}_\varphi$, which leads to a closed equation of motion for α. If we account for fluctuations, e.g. due to thermal noise in the resonator, α becomes a stochastic variable obeying a Langevin equation [44],

$$\dot{\alpha} = \left[\frac{C}{\tilde{\Gamma}_\varphi + i\delta\Omega} s_z^{st} - \kappa - 4ig_3 s_z^{st}\right]\frac{\alpha}{2} + \xi(t)\,. \tag{23}$$

Here $C \equiv 2g_1^2$, and $s_z^{st} = -D_0/(1 + |\alpha^2|/\tilde{n}_0)$ is the stationary value of the population difference between the qubit levels, with $D_0 = (\tilde{\Gamma}_\downarrow - \tilde{\Gamma}_\uparrow)/\tilde{\Gamma}_1$ being the normalized difference between the rates with $\tilde{\Gamma}_1 = \tilde{\Gamma}_\uparrow + \tilde{\Gamma}_\downarrow$. Furthermore, $\tilde{\Gamma}_\varphi = \tilde{\Gamma}_1/2 + \tilde{\Gamma}_\varphi^*$ is the total dephasing rate. The detuning of the Rabi frequency enters in combination with a frequency renormalization, $\delta\Omega \equiv \Omega_R - \omega_T + g_3|\alpha|^2$. We further introduced the photon saturation numbers $n_0 = \tilde{\Gamma}_\varphi \tilde{\Gamma}_1/4g_1^2$ and $\tilde{n}_0 \equiv n_0(1 + \delta\Omega^2/\tilde{\Gamma}_\varphi^2)$.

As one can see from equation (23) the driving increases the photon number $n = |\alpha|^2$. Once it reaches $\tilde{n}_0$ the qubit's negative contribution to the oscillator's effective friction coefficient starts to diminish and, finally, causes the saturation of n. The saturation number is easiest to understand in the framework of the Jaynes–Cummings spectrum, i.e. the spectrum of a coupled system consisting of a two-level system and an oscillator at resonance with each other. The coupling lifts the degeneracy between the states $|\uparrow, n\rangle$ and $|\downarrow, n+1\rangle$ and creates an energy splitting of order $g_1\sqrt{n}$. Once the occupation number n reaches the saturation number n_0 the energy splitting $g_1\sqrt{n}$ becomes larger than the rate Γ_1 which, in the case of population inversion, serves also as the pumping rate. At this stage, the pumping becomes ineffective and the growth of n slows down and for still larger photon numbers stops.

The Langevin force $\xi = \xi_{osc} + \xi_{qb}$ arises due to the thermal noise of the oscillator's dissipative environment, ξ_{osc}, as well as the noise of the driven qubit, ξ_{qb}. By the fluctuation dissipation theorem, the former satisfies $\langle \xi_{osc}(t)\xi_{osc}^*(t')\rangle = \kappa N_{th}\delta(t - t')$ and $\langle \xi_{osc}(t)\xi_{osc}(t')\rangle = 0$.

The noise originating from the qubit can be estimated as $\langle \xi_{\rm qb}(t)\xi^*_{\rm qb}(t')\rangle = (g_1^2/\tilde{\Gamma}_\varphi)\delta(t-t')$ and $\langle \xi_{\rm qb}(t)\xi_{\rm qb}(t')\rangle = 0$. Provided the oscillator's thermal noise is strong, i.e. if $\kappa N_{\rm th} \gg g_1^2/\tilde{\Gamma}_\varphi$, the qubit's noise can be neglected compared to the former.

2.4.2. Two-photon interaction. The two-photon effect dominates near the resonance $\Omega_{\rm R} \approx 2\omega_{\rm T}$. In RWA, the Hamiltonian reduces to

$$H_{\rm I} = g_2\left(a^{\dagger 2}\sigma_- {\rm e}^{-{\rm i}(\Omega_{\rm R}-2\omega_{\rm T})t} + {\rm h.c.}\right) + g_3\left(a^\dagger a + aa^\dagger\right)\sigma_z. \tag{24}$$

The corresponding Langevin equation for the resonator variable reads

$$\dot{\alpha} = \left[\frac{C}{\tilde{\Gamma}_\varphi + {\rm i}\delta\Omega}s_z^{\rm st} - \kappa - 4{\rm i}g_3 s_z^{\rm st}\right]\frac{\alpha}{2} + \xi(t), \tag{25}$$

i.e. it is of the same form as equation (23) except that $C \equiv 4g_2^2|\alpha|^2$ and $s_z^{\rm st} = -D_0/(1+(|\alpha^2|/\tilde{n}_0)^2)$. The photon saturation number is now given by $n_0 = (\tilde{\Gamma}_\varphi\tilde{\Gamma}_1/4g_2^2)^{1/2}$ and $\tilde{n}_0 \equiv n_0(1+\delta\Omega^2/\tilde{\Gamma}_\varphi^2)^{1/2}$. The detuning of the Rabi frequency for two-photon interaction is given by $\delta\Omega \equiv \Omega_{\rm R} - 2\omega_{\rm T} + g_3|\alpha|^2$. Again $\xi(t)$ is mostly due to the thermal noise, while noise arising from the qubit can be neglected if $\kappa N_{\rm th} \gg g_2^2\bar{n}/\tilde{\Gamma}_\varphi$.

3. Results

3.1. Results obtained from the Langevin equation

If one neglects the frequency shifts of the oscillator, i.e. for $g_3 = 0$, the Fokker–Planck equations corresponding to the Langevin equations (23) and (25) have exact analytic solutions [45]. Also for $g_3 \neq 0$ the equations (23) and (25) written as $\dot{\alpha} = -f(n)\alpha/2 + \xi(t)$ can be transformed into equations for the average number of photons $\langle|\alpha|^2\rangle = \bar{n}$ in the form $\dot{\bar{n}} = -\langle n{\rm Re}[f(n)]\rangle + \kappa N_{\rm th}$. In the steady state, for $\bar{n} \gg 1$ they can be approximated by $\bar{n}{\rm Re}[f(\bar{n})] = \kappa N_{\rm th}$. The results of this analysis are shown in figure 3. To demonstrate both the one-photon and the two-photon effects, we assumed that the qubit is biased sightly off the symmetry point, $\epsilon = 0.01\Delta$. The two-photon resonance (the outer one) persists for $\epsilon = 0$, whereas the one-photon resonance (the inner one) vanishes there. We observe that the solution shows bistability bifurcations [46] (see below). As a result, we see in figure 3 sharp drops of $\bar{n}$ for both resonances as only the lowest stable value is plotted.

In the lasing regime, we can estimate the asymptotic solutions analytically. In the one-photon case, assuming $\bar{n} \gg \tilde{n}_0$, we obtain from equation (23)

$$\bar{n} \sim N_{\rm th} + \frac{(-D_0)\tilde{\Gamma}_1}{2\kappa}. \tag{26}$$

This result holds independent of whether the second contribution due to the qubit is larger or smaller than the thermal number $N_{\rm th}$ as long as $\bar{n} \gg \tilde{n}_0$. In the two-photon case, assuming $\bar{n} \gg \tilde{n}_0$, we obtain from equation (25)

$$\bar{n} \sim N_{\rm th} + \frac{(-D_0)\tilde{\Gamma}_1}{\kappa}. \tag{27}$$

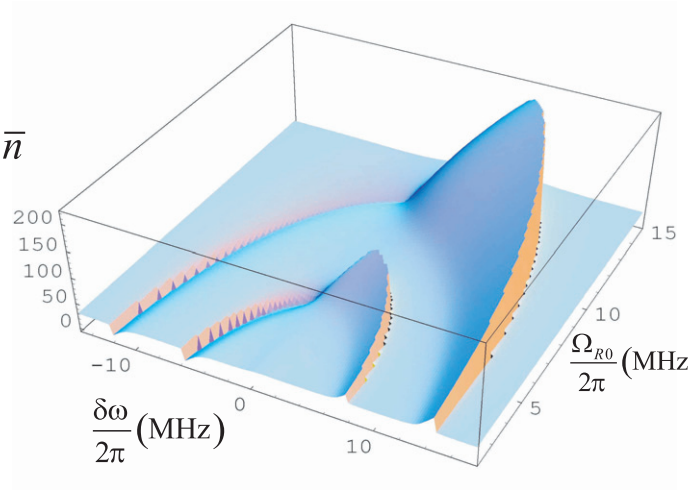

Figure 3. Average number of photons in the resonator as a function of the driving detuning $\delta\omega$ and amplitude Ω_{R0}. Peaks at $\delta\omega > 0$ correspond to lasing, while dips at $\delta\omega < 0$ correspond to cooling. The inner curve corresponds to the one-photon resonance which exists only away from the symmetry point. Here, we assumed $\epsilon = 0.01\Delta$. The outer curve describes the two-photon resonance, which persists at $\epsilon = 0$. In domains of bistability the lowest value of $\bar{n}$ is plotted (leading to the sharp drops in both curves). We chose the following parameters for the qubit: $\Delta/2\pi = 1\,\text{GHz}$, $\epsilon = 0.01\Delta$, $\Gamma_0/2\pi = 125\,\text{kHz}$, the resonator: $\omega_T/2\pi = 6\,\text{MHz}$, $\kappa/2\pi = 0.34\,\text{kHz}$, and the coupling: $g/2\pi = 3.3\,\text{MHz}$. The bath temperature is $T = 10\,\text{mK}$.

3.2. Solution of the master equation

We also solved the full master equation (19) numerically, which provides access not only to the average number of photons in the oscillator, $\bar{n}$, but also to the whole distribution function $P(n)$. Assuming a low thermal number, $N_{\text{th}} = 5$ and a relatively high relaxation constant of the oscillator $\kappa/2\pi = 1.7\,\text{kHz}$, we reach convergence with a limited number of photon basis states ($n \leqslant 100$). In figure 4, the solutions of the Langevin equations (23) and (25) and those of the master equation (19) are compared. By construction, the solution of the master equation (19) provides the uniquely defined stationary distribution function for the occupation number $P(n)$. Thus, the average occupation number defined as $\bar{n} = \sum_n nP(n)$ is also uniquely defined and is plotted in figure 4. In contrast, the Langevin equations (23) or (25) yield in a certain interval of parameters two stable solutions for $\bar{n} = |\alpha|^2$, as shown in figure 4. We observe that in regimes of single stability the solutions of the master equation and of the Langevin equations agree very well. In the bistability regime, the master equation produces approximately the average between the two stable solutions of the Langevin equation. This indicates that in the bistability regime, the system switches between the two stable states. Further indications of this 'telegraph' behavior are obtained from the analysis of the Fano factor.

In figure 5, the Fano factor $F = (\langle n^2\rangle - \langle n\rangle^2)/\langle n\rangle$ of the photon number distribution is presented. We observe two phenomena. First, in the regime of lasing without bistability, the Fano factor is reduced as compared to that of the thermal state. Indeed, the Fano factor in the

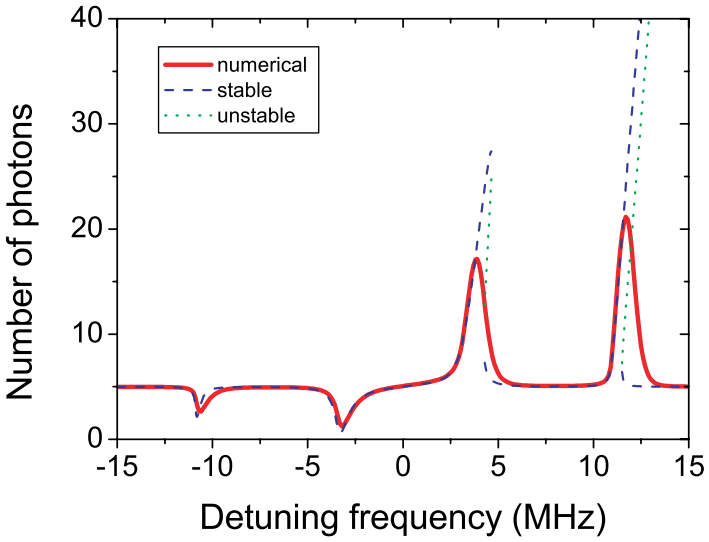

Figure 4. Average number of photons $\bar{n}$ versus the detuning. The blue dashed and the green dotted curves are obtained from the Langevin equations (23) and (25). They show the bistability with the blue dashed curve denoting stable solutions, whereas the green dotted curve denotes the unstable solution. The red solid curve is obtained from a numerical solution of the master equation (19). The driving amplitude is taken as $\Omega_{R0}/2\pi = 5\,\mathrm{MHz}$. The parameters of the qubit: $\Delta/2\pi = 1\,\mathrm{GHz}$, $\epsilon = 0.01\Delta$, $\Gamma_0/2\pi = 125\,\mathrm{kHz}$, the resonator: $\omega_T/2\pi = 6\,\mathrm{MHz}$, $\kappa/2\pi = 1.7\,\mathrm{kHz}$, $N_{th} = 5$, and the coupling: $g/2\pi = 3.3\,\mathrm{MHz}$.

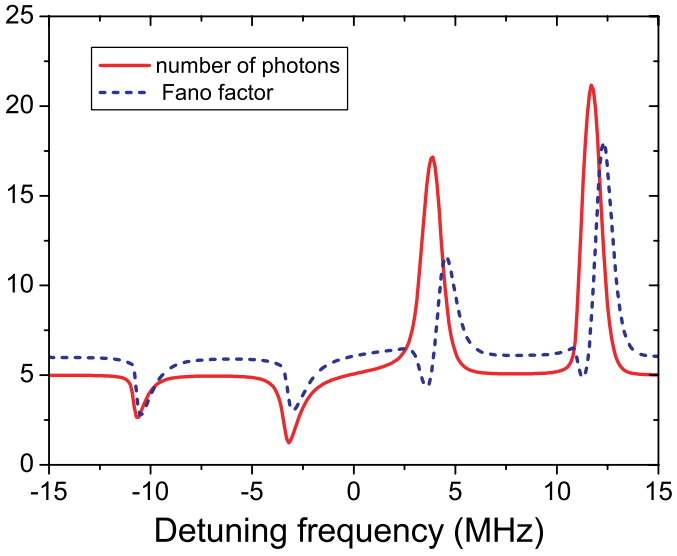

Figure 5. The Fano factor (dashed blue), and the average photon number $\bar{n}$ (solid red). The parameters are as in figure 4.

ideal lasing state should approach 1, down from the thermal value $N_{th} + 1$. In contrast, in the bistable regime the Fano factor increases. We interpret this result as another indication of the switching between the two stable solutions. In the cooling regime, the Fano factor, as expected, follows the effective temperature of the oscillator, i.e. is reduced.

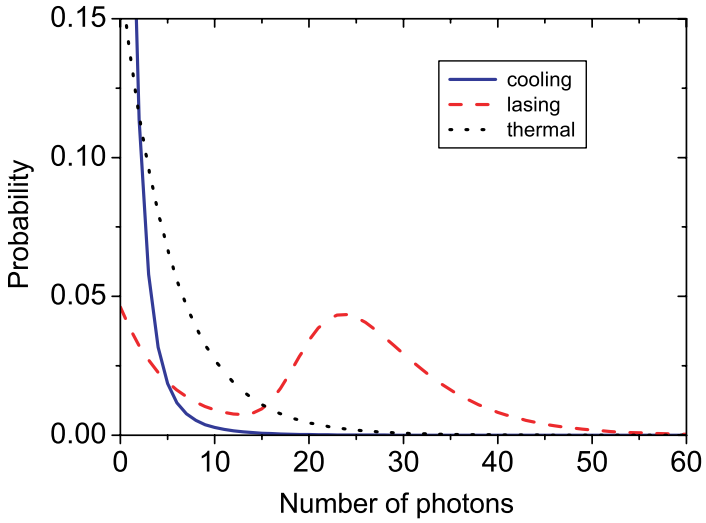

Figure 6. The distribution function, $P(n)$, obtained by numerically solving the master equation (19). Blue solid curve: cooling regime of the one-photon resonance with $\Omega_{R0} = 2\pi \times 5\,\mathrm{MHz}$ and $\delta\omega = -2\pi \times 3.2\,\mathrm{MHz}$. Red dashed curve: lasing regime of the two-photon resonance with $\Omega_{R0} = 2\pi \times 5\,\mathrm{MHz}$ and $\delta\omega = 2\pi \times 11.7\,\mathrm{MHz}$. We observe a peak in the $P(n)$ distribution between $n = 20$ and 30 as a result of the lasing behavior. Black dotted curve: thermal distribution with $N_{\mathrm{th}} = 5$. The parameters are as in figure 4.

In figure 6, the distribution function, $P(n)$, for the number of photons in the oscillator is plotted both for the cooling and lasing regimes. For comparison, also the thermal (Bose–Einstein) distribution is plotted. We observe that in the lasing regime, the distribution function combines the Poisson-like part and the thermal-like one. This is yet another indication of the bistability. On the other hand, in the cooling regime the distribution function is thermal-like with the reduced effective temperature.

The lasing and cooling effects described here rely crucially on the transition rates, as described by the Liouville equations. In order to demonstrate this dependence, we plot in figure 7 the average photon number versus the qubit's relaxation rate at the one-photon resonance. We note a non-monotonic dependence. This behavior is explained by the dependence of the saturation number n_0 on Γ_0 indicated in figure 7. While n_0 grows quadratically with Γ_0 the average occupation number $\bar{n}$ grows only linearly, cf equations (26) and (27). This regime holds as long as $\bar{n} > n_0$. Indeed, in this regime the pumping rate is limited by Γ_0, leading to a roughly linear growth of the photon number with increasing Γ_0, consistent with equations (26) and (27). Once the saturation threshold is reached, $\bar{n} \sim n_0$, the effective coupling $\sim g_1\sqrt{\bar{n}}$ becomes comparable to Γ_0 and the photon number becomes insensitive to small variations of Γ_0. Since the saturation number n_0 continues to grow, the regime $\bar{n} < n_0$ is reached. In this case, a further increase of Γ_0 predominantly increases the dephasing rate $\tilde{\Gamma}_\varphi$. As can be seen from equation (23) this reduces the effect of the qubit on the oscillator and the photon number decreases towards N_{th}. In figure 7, we plot both the results of a numerical solution of the master equation and of the Langevin equation. We find a good agreement between the two.

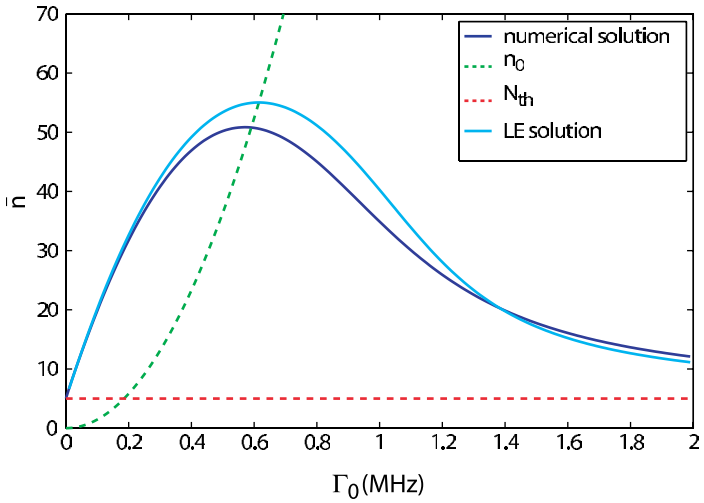

Figure 7. Average number of photons in the resonator as a function of the qubit's relaxation rate, Γ_0 at the one-photon resonance, $\Omega_R = \omega_T$ for $g_3 = 0$ and $N_{th} = 5$. The dark blue line shows the numerical solution of the master equation, the light blue solid line represents the solution of the Langevin equation, equation (23). The green and red dashed curves represent, respectively, the saturation number n_0 and the thermal photon number N_{th}. The parameters are as in figure 4 (except for Γ_0).

4. Discussion

We summarize our main conclusions. Our results for the number of photons $\bar{n}$ are plotted in figure 3 as a function of the detuning $\delta\omega$ of the driving frequency and driving amplitude Ω_{R0}. It exhibits sharp structures along two curves corresponding to the one- and two-photon resonance conditions, $\Omega_R = \omega_T - g_3\bar{n}$ and $\Omega_R = 2\omega_T - g_3\bar{n}$. Blue detuning, $\delta\omega > 0$, induces a strong population inversion of the qubit levels, which in resonance leads to one-qubit lasing. In experiments the effect can be measured as a strong increase of the number of photons in the resonator above the thermal values. Red detuning produces a one-qubit cooler with resulting photon numbers substantially below the thermal value.

The bistability of the solution of the Langevin description is illustrated in figure 4. In the range of bistability, we expect a telegraph-like noise corresponding to the random switches between the two solutions.

Potentially useful applications of the considered scheme are the lasing behavior and the creation of a highly non-thermal population of the oscillator as well as the cooling. Within the accuracy of our approach, we estimate that a population of order $\bar{n} = 1$ can be reached for optimal detuning.

So far we have described an LC-oscillator coupled to a flux qubit. But our analysis equally applies for a nanomechanical resonator coupled capacitively to a Josephson charge qubit [6] (see figure 1(b)). In this case, σ_z stands for the charge of the qubit and both the coupling to the oscillator as well as the driving are capacitive, i.e. involve σ_z. To produce the capacitive coupling between the qubit and the oscillator, the latter could be metal-coated and charged by the voltage source V_x. The dc component of the gate voltage V_g puts the system near the charge

degeneracy point, where the dephasing due to the $1/f$ charge noise is minimal. Rabi driving is induced by an ac component of V_g. Realistic experimental parameters are expected to be very similar to the ones used in the examples discussed above, except that a much higher quality factor of the resonator ($\sim 10^5$) and a much higher number of quanta in the oscillator can be reached. This number will easily exceed the thermal one, thus a proper lasing state with Poisson statistics, appropriately named SASER [29], is produced. One should then observe the usual line narrowing [44] with line width given by $\kappa N_{\rm th}/(4\bar{n}) \sim \kappa^2 N_{\rm th}/\tilde{\Gamma}_1$. Experimental observation of this line-width narrowing would constitute a confirmation of the lasing/sasing.

In experiments with the same setup as shown in figure 1(a)—but in a different parameter regime when the relaxation rate of the qubit is close to the oscillator's frequency—the mechanisms of *Sisyphus* cooling and amplification have recently been demonstrated [7]. In these experiments, the LC tank circuit is driven near-resonantly by a low-frequency ac current, and its response, which is influenced by the high-frequency driven qubit, is detected. For red-detuned high-frequency driving of the qubit the low-frequency LC-circuit carries out work in its forward and backward oscillation cycle, always increasing the energy of the qubit (similar to Sisyphus always pushing up a rock). This produces additional damping and a reduction of the effective quality factor, which can be associated with cooling of the oscillator. For blue-detuned qubit driving, the same mechanism leads to Sisyphus amplification ('lucky Sisyphus' rolling the rock down) and a precursor of lasing of the resonator. It is accompanied by an enhancement of the effective quality factor. These effects were confirmed in the second series of experiments where the power spectrum of the oscillator, i.e. the number of photons and the line-width, were measured directly. A quantitative analysis [7] in the frame of the theory outlined in this paper confirms this picture and allows parameter regimes to be identified where these effects are optimized.

Acknowledgments

We thank E Il'ichev, O Astafiev, A Blais, M Devoret, D Esteve, M D LaHaye, M Marthaler, Y Nakamura, F Nori, E Solano, K C Schwab and F K Wilhelm for fruitful discussions. The work is part of the EU IST Project EuroSQIP.

References

[1] Il'ichev E, Oukhanski N, Izmalkov A, Wagner Th, Grajcar M, Meyer H-G, Smirnov A Yu, van den Brink A M, Amin M H S and Zagoskin A M 2003 Continuous monitoring of Rabi oscillations in a Josephson flux qubit *Phys. Rev. Lett.* **91** 097906

[2] Wallraff A, Schuster D I, Blais A, Frunzio L, Huang R-S, Majer J, Kumar S, Girvin S M and Schoelkopf R J 2004 Circuit quantum electrodynamics: coherent coupling of a single photon to a Cooper pair box *Nature* **431** 162

[3] Chiorescu I, Bertet P, Semba K, Nakamura Y, Harmans C J P M and Mooij J E 2004 Coherent dynamics of a flux qubit coupled to a harmonic oscillator *Nature* **431** 159

[4] Wallraff A, Schuster D I, Blais A, Frunzio L, Majer J, Devoret M H, Girvin S M and Schoelkopf R J 2005 Approaching unit visibility for control of a superconducting qubit with dispersive readout *Phys. Rev. Lett.* **95** 060501

[5] Johansson J, Saito S, Meno T, Nakano H, Ueda M, Semba K and Takayanagi H 2006 Vacuum Rabi oscillations in a macroscopic superconducting qubit LC oscillator system *Phys. Rev. Lett.* **96** 127006

[6] Naik A, Buu O, LaHaye M D, Armour A D, Clerk A A, Blencowe M P and Schwab K C 2006 Cooling a nanomechanical resonator with quantum back-action *Nature* **443** 193
[7] Grajcar M, van der Ploeg S H W, Izmalkov A, Il'ichev E, Meyer H G, Fedorov A, Shnirman A and Schön G 2008 Sisyphus cooling and amplification by a superconducting qubit *Nat. Phys.* **4** 612
[8] Deppe F *et al* 2008 Two-photon probe of the Jaynes–Cummings model and symmetry breaking in circuit QED arXiv:0805.3294
[9] Buisson O, Balestro F, Pekola J P and Hekking F W J 2003 One-shot quantum measurement using a hysteretic dc SQUID *Phys. Rev. Lett.* **90** 238304
[10] Blais A, Huang R S, Wallraff A, Girvin S M and Schoelkopf R J 2004 Cavity quantum electrodynamics for superconducting electrical circuits: an architecture for quantum computation *Phys. Rev.* A **9** 062320
[11] Liu Y X, Wei L F and Nori F 2004 Generation of nonclassical photon states using a superconducting qubit in a microcavity *Europhys. Lett.* **67** 941
[12] Martin I, Shnirman A, Tian L and Zoller P 2004 Ground state cooling of mechanical resonators *Phys. Rev.* B **69** 125339
[13] Moon K and Girvin S M 2005 Theory of microwave parametric down-conversion and squeezing using circuit QED *Phys. Rev. Lett.* **95** 140504
[14] Mariantoni M, Storcz M J, Wilhelm F K, Oliver W D, Emmert A, Marx A, Gross R, Christ H and Solano E 2005 On-chip microwave fock states and quantum homodyne measurements arXiv:cond-mat/0509737
[15] Liu Y X, Sun C P and Nori F 2006 Scalable superconducting qubit circuits using dressed states *Phys. Rev.* A **74** 052321
[16] Wallquist M, Shumeiko V S and Wendin G 2006 Selective coupling of superconducting qubits via tunable stripline cavity *Phys. Rev.* B **74** 224506
[17] Xue F, Wang Y D, Sun C P, Okamoto H, Yamaguchi H and Semba K 2007 Controllable coupling between flux qubit and nanomechanical resonator by magnetic field *New J. Phys.* **9** 35
[18] Hauss J, Fedorov A, Hutter C, Shnirman A and Schön G 2008 Single-qubit lasing and cooling at the Rabi frequency *Phys. Rev. Lett.* **100** 037003
[19] Ashhab S, Johansson J R, Zagoskin A M and Nori F 2008 Single-artificial-atom lasing and its suppression by strong pumping arXiv:0803.1209
[20] Smirnov A Yu 2003 Theory of weak continuous measurements in a strongly driven quantum bit *Phys. Rev.* B **68** 134514
[21] Greenberg Ya S, Il'ichev E and Izmalkov A 2005 Low frequency Rabi spectroscopy for a dissipative two-level system *Europhys. Lett.* **72** 880
[22] Mu Y and Savage C M 1992 One-atom lasers *Phys. Rev.* A **46** 5944–54
[23] McKeever J, Boca A, Boozer A D, Buck J R and Kimble H J 2003 Experimental realization of a one-atom laser in the regime of strong coupling *Nature* **425** 268
[24] Zakrzewski J, Lewenstein M and Mossberg T W 1991 Theory of dressed-state lasers. I. Effective Hamiltonians and stability properties *Phys. Rev.* A **44** 7717
[25] Mollow B R 1969 Power spectrum of light scattered by two-level systems *Phys. Rev.* **188** 1969–75
[26] Stace T M, Doherty A C and Barrett S D 2005 Population inversion of a driven two-level system in a structureless bath *Phys. Rev. Lett.* **95** 106801
[27] Jonathan D and Plenio M B 2001 Light-shift-induced quantum gates for ions in thermal motion *Phys. Rev. Lett.* **87** 127901
[28] Jaehne K, Hammerer K and Wallquist M 2008 Ground state cooling of a nanomechanical resonator via a Cooper pair box qubit arXiv:0804.0603
[29] Kent A J, Kini R N, Stanton N M, Henini M, Glavin B A, Kochelap V A and Linnik T L 2006 Acoustic phonon emission from a weakly coupled superlattice under vertical electron transport: observation of phonon resonance *Phys. Rev. Lett.* **96** 215504
[30] Fulton T A, Gammel P L, Bishop D J, Dunkleberger L N and Dolan G J 1989 Observation of combined Josephson and charging effects in small tunnel junction circuits *Phys. Rev. Lett.* **63** 1307

[31] Maassen van den Brink A, Schön G and Geerligs L J 1991 Combined single electron and coherent Cooper pair tunneling in voltage-biased Josephson junctions *Phys. Rev. Lett.* **67** 3030
[32] Maassen van den Brink A, Odintsov A A, Bobbert P A and Schön G 1991 Coherent Cooper pair tunneling in systems of Josephson junctions: effects of quasiparticle tunneling and of the electromagnetic environment *Z. Phys.* B **85** 459
[33] Blanter Ya M, Usmani O and Nazarov Yu V 2004 Single-electron tunneling with strong mechanical feedback *Phys. Rev. Lett.* **93** 136802
[34] Blencowe M P, Imbers J and Armour A D 2005 Dynamics of a nanomechanical resonator coupled to a superconducting single-electron transistor *New J. Phys.* **7** 236
[35] Clerk A A and Bennett S 2005 Quantum nano-electromechanics with electrons, quasiparticles and Cooper pairs: effective bath descriptions and strong feedback effects *New J. Phys.* **7** 238
[36] Bennett S D and Clerk A A 2006 Laser-like instabilities in quantum nano-electromechanical systems *Phys. Rev.* B **74** 201301
[37] Usmani O, Blanter Ya M and Nazarov Yu V 2007 Strong feedback and current noise in nanoelectromechanical systems *Phys. Rev.* B **75** 195312
[38] Rodrigues D A, Imbers J and Armour A D 2007 Quantum dynamics of a resonator driven by a superconducting single-electron transistor: a solid-state analogue of the micromaser *Phys. Rev. Lett.* **98** 067204
[39] Astafiev O, Inomata K, Niskanen A O, Yamamoto T, Pashkin Yu A, Nakamura Y and Tsai J S 2007 Single artificial-atom laser *Nature* **449** 588–90
[40] Greenberg Ya S, Izmalkov A, Grajcar M, Il'ichev E, Krech W, Meyer H-G, Amin M H S and van den Brink A M 2002 Low-frequency characterization of quantum tunneling in flux qubits *Phys. Rev.* B **66** 214525
[41] Bloch F 1957 Generalized theory of relaxation *Phys. Rev.* **105** 1206
[42] Redfield A G 1957 On the theory of relaxation processes *IBM J. Res. Dev.* **1** 19
[43] Ithier G *et al* 2005 Decoherence in a superconducting quantum bit circuit *Phys. Rev.* B **72** 134519
[44] Gardiner C W and Zoller P 2004 *Quantum Noise* 3rd edn (Berlin: Springer)
[45] Reid M, McNeil K J and Walls D F 1981 Unified approach to multiphoton lasers and multiphoton bistability *Phys. Rev.* A **24** 2029
[46] Drummond P D and Walls D F 1980 Quantum theory of optical bistability. I. Nonlinear polarisability model *J. Phys. A: Math. Gen.* **13** 725